Many-Body Effects in fcc Metals: A Lennard-Jones Embedded-Atom Potential

M. I. Baskes*
Sandia National Laboratories, Livermore, California 94551-0969
(Received 16 February 1999)

A simple analytic model that extends the Lennard-Jones potential into the many-body regime is proposed. The two parameter model draws on the embedded-atom method formalism. The model is used to calculate properties of an fcc material, e.g., elastic constants, Bain transformation, and defect properties, as a function of many-body parameters. It is shown that the ground state structure of the model includes all of the common phases. The melting point of an fcc material is shown to decrease significantly as the many-body interactions are increased.

PACS numbers: 61.50.Lt, 62.20.Dc, 64.70.Dv, 64.70.Kb

The Lennard-Jones (LJ) potential [1] is one of the oldest interatomic potentials in the literature. This potential has been used to model a wide range of materials and phases, ranging from rare gas solids to metallic liquids [2,3]. More recently there has been renewed interest in homogeneous nucleation from a LJ liquid [4–7], the dynamics of diffusion in liquids and solids [8], and equilibrium structures in supercooled liquids [9,10]. Many calculations have been performed to examine free surfaces [11] and grain boundaries [12] in LJ materials. LJ potentials have recently been used to model the fracture process in two dimensional solids [13] and in quasicrystals [14]. There is a vast database of knowledge available in the literature about the behavior of LJ materials. Of course, the interactions in real materials are more complex than that described by a simple pair interaction. In the past fifteen years it has become well accepted that many-body effects play an important role in the behavior of materials, especially metals and alloys [15]. Recognizing the need for many-body interactions, Daw and Baskes [16,17] developed the embedded-atom method (EAM) to treat metallic systems. The theory behind EAM and many applications have recently been reviewed [18]. The purpose of this Letter is to present a very simple extension of the LJ potential to allow investigation of many-body effects. A model based on this concept was previously presented by Holian *et al.* [19]. This extension provides a simple analytic model that appears to be extremely rich in opportunity.

Let us start with an expression for the energy of bond in a material described by the Lennard-Jones form,

$$\phi_{\mathrm{LJ}} = \frac{1}{r^{12}} - \frac{2}{r^{6}}, \tag{1}$$

where the energy is measured in units of the well depth, ε, and the atomic separation, r, is measured in units of $r_0 = 2^{1/6}\sigma$, where σ is the LJ diameter. For an equilibrium fcc material with only $Z_0 = 12$ nearest neighbor interactions, the scaled energy is equal to $-Z_0/2$, and the scaled equilibrium nearest neighbor distance is unity. Using this bond energy relationship and the nearest neighbor fcc structure as a reference state, we may define a simple EAM model for the total energy of an arbitrary arrangement of atoms [20],

$$E = \sum_i \left[F(\overline{\rho}_i) + \frac{1}{2}\sum_{j\neq i}\phi(r_{ij}) \right], \tag{2a}$$

$$F(\overline{\rho}) = \frac{AZ_0}{2}\,\overline{\rho}[\ln(\overline{\rho}) - 1], \tag{2b}$$

$$\phi(r) = \phi_{\mathrm{LJ}}(r) - \frac{2}{Z_0}F(\rho(r)), \tag{2c}$$

$$\overline{\rho}_i = \frac{1}{Z_0}\sum_{j\neq i}\rho(r_{ij}), \tag{2d}$$

$$\rho(r) = \exp[-\beta(r - 1)], \tag{2e}$$

where the sums are over the j neighbors of an atom i, and r_{ij} is the distance between the two atoms. The embedding energy in Eq. (2b) is taken as a form motivated by Pauling [21] and reproduces the classical bond energy, distance, and coordination relationship [22]. The background electron density $\overline{\rho}$ is given by the usual linear superposition of atomic densities ρ. We have introduced two dimensionless parameters into the model: the extent of the many-body bonding, quantified by the parameter A, and the decay of the electron density, quantified by the parameter β. Note that the model reduces to a LJ solid for $A = 0$ and any value of β. The model is presented for a single component material, but is easily extended to multicomponent systems.

Using this simple model we may now examine how properties of our fcc solid vary with the extent of the many-body term (Table I). By our choice of the LJ potential as a model of the reference fcc lattice, the bulk modulus B, normalized by the LJ well depth ε, the atomic volume $\Omega = r_0^3/\sqrt{2}$, and the elastic anisotropy are forced to be the same in the LJ and EAM-LJ models. Even though the ratio of the shear elastic constants is independent of the many-body interactions, the actual elastic shear constants are reduced as the many-body term increases. The Cauchy discrepancy, which of course is zero for a pair potential, increases with the strength of the many-body term. Similarly the unrelaxed vacancy formation energy and surface energy [given here for a (100) surface] are reduced as the many-body interactions increase. The

 0031-9007/99/83(13)/2592(4)$15.00

TABLE I. Comparison of LJ, EAM-LJ, and experimental normalized properties for fcc materials. The first column under EAM-LJ gives the analytic expression, the second gives the calculated range of values using the range of A and β investigated in this Letter.

Property		LJ	EAM-LJ		Experiment	
					Rare Gas	Metal
Bulk modulus	$B\Omega/\varepsilon$	48	48	48	52–58	14–28
Elastic anisotropy	$2c_{44}/(c_{11} - c_{12})$	2	2	2	2.3–2.4	1.2–4.0
Elastic shear	c_{44}/B	0.75	$3/4\ (1 - A\beta^2/72)$	0–0.75	0.74–0.83	0.3–0.7
Cauchy discrepancy	$(c_{12} - c_{44})/B$	0	$A\beta^2/72$	0–0.8	−0.06–0.05	−0.4–0.7
Vacancy energy	E_{1v}^f/ε	6	$6\ (1 - 0.96A)$	0–6	4.0–5.7	1.2–3.0
Surface energy	$E_{\text{surf}}r_0^2/\varepsilon$	2	$2\ (1 - 0.83A)$	0–2		0.9–1.4

decrease in surface energy for the (111) and (110) surfaces is almost identical to that of the (100) surface.

Let us now relate the model properties to real materials. The final two columns of Table I give the range of normalized properties for the rare gases and the 10 fcc materials discussed in Ref. [20]. Here we see that the LJ (and EAM-LJ) model has a bulk modulus significantly greater than the fcc metals. The LJ model yields a bulk modulus about 15% lower than the experimental rare gas moduli. On the other hand, the anisotropy ratio falls about in the middle of the range of the fcc materials and within 20% for the rare gases. The elastic shear modulus from LJ is at the top of the experimental range for the fcc materials and is quite accurate for the rare gases, but the addition of the many-body term reduces the shear modulus into the range of the fcc materials. For the rare gases the Cauchy discrepancy is nearly zero and is modeled well by a pair potential. As expected the EAM-LJ model can have a positive Cauchy discrepancy in agreement with most of the fcc materials, but only the addition of angular forces can reproduce the negative Cauchy discrepancies seen in a small number of fcc metals. It is well known that the vacancy formation energy calculated from a pair potential is significantly higher than experiment even for a rare gas solid. Addition of the many-body interactions reduces this energy to be more in agreement with experiment. The surface energy from pair potentials is in much better agreement with experiment, albeit somewhat high. Again the many-body term reduces the surface energy. However, since the vacancy formation and surface energy are strongly correlated (see the analytic expression in Table I), we see why typical EAM functions, which fit the vacancy formation energy, underestimate the surface energy.

It is also of interest to examine the behavior of crystal structures other than fcc. For simplicity here, we will consider a small number of high symmetry atomic arrangements, i.e., fcc, bcc, simple cubic (sc), diamond cubic (dc), graphite sheets, and a dimer. The structures were chosen to include a large range of coordination, ranging from 1 for the dimer to 12 for fcc. In Table II we see that the structural energy for the LJ model depends rather sensitively on the inclusion of second neighbors, especially for the bcc and sc structures. This effect occurs because for bcc, the second neighbor distance is very close to the first neighbor distance, while for sc there are twice as many second neighbors as first neighbors. Thus the following calculations are performed including second neighbors for all structures.

For each structure the energy per atom was calculated at zero pressure by minimizing the energy with respect to the nearest neighbor distance. The results of the calculations for the EAM-LJ model are presented in Fig. 1 as a phase stability diagram. For this second neighbor model the ground state using simply the LJ potential is the fcc structure. Note that for a second neighbor model the ideal hcp and fcc structural energies are identical. Thus we observe that the ground state is fcc for low values of the parameter A. We see that as the many-body interactions are increased, the ground state changes from fcc to the lower coordinated structures in a very regular fashion. For the smaller values of β, i.e., a long range electron density, the bcc structure is favored. The progression towards the lowest coordinated states (dimer) is facilitated by a shorter range electron density.

It is interesting to investigate the transitions from one phase to another. A recent Letter [23] described first principles local density approximation calculations of the Bain tetragonal distortion taking a crystal between the fcc and bcc structures. These calculations showed that the phase with the higher energy was unstable with respect to the Bain distortion, even though it was stable with respect to a cubic distortion. Using the EAM-LJ model and considering interactions to second neighbors, we have calculated the structural energy as a function of Bain distortion for three cases. The first case is simply the

TABLE II. Number of first (Z_1) and second (Z_2) neighbors for various structures. The ratio of the second neighbor distance (r_2) to first neighbor distance (r_1) and the ratio of the LJ energy considering up to second neighbor interactions (E_2) to the energy considering only first neighbor interactions (E_1) are also given.

	Z_1	Z_2	r_2/r_1	E_2/E_1
fcc	12	6	$\sqrt{2}$	1.1
bcc	8	6	$\sqrt{4/3}$	1.5
sc	6	12	$\sqrt{2}$	1.5
dc	4	12	$\sqrt{8/3}$	1.3
Graphite	3	6	$\sqrt{3}$	1.1
Dimer	1	...	...	...

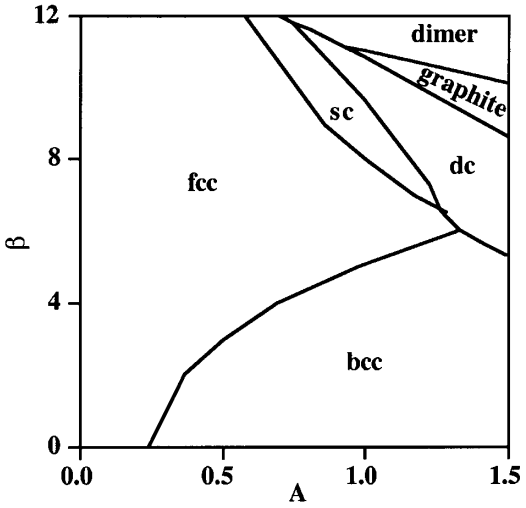

FIG. 1. Ground state structure as a function of the model parameters A and β.

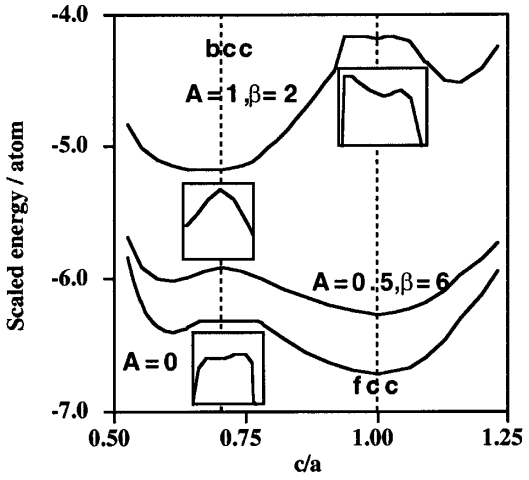

FIG. 2. Scaled energy vs the c/a ratio for the tetragonal Bain transformation. Three cases are shown, representing the LJ model ($A = 0$) and two EAM-LJ models. The fcc structure occurs at $c/a = 1$ and the bcc at 0.707. Insets show the detail of the higher energy phase.

LJ pair model ($A = 0$) which has the fcc phase more stable than the bcc phase. The other two cases have a varying amount of many-body contribution that was chosen (see Fig. 1) so that the fcc phase is stable in one case ($A = 0.5, \beta = 6$) and the bcc phase, in the other ($A = 1, \beta = 2$). The results are shown in Fig. 2. The energy is calculated for a fixed c/a ratio and variable volume, which is chosen to produce a minimum energy. For the case of pure pair potential ($A = 0$) the bcc phase is actually at a very shallow metastable minimum and for the many-body case, the fcc phase is at a maximum. On the other hand, when bcc is the lower energy phase, the fcc phase has a very shallow minimum. It is quite encouraging that a model as simple as EAM-LJ is able to reproduce the behavior seen in the first principles calculations.

The melting of LJ solids is one of the most widely studied phenomena in model systems. The calculated melting point depends weakly on the interaction range and is approximately given by $kT_m/\varepsilon = 0.7$ [24]. This melting point is in reasonable agreement with the experimental melting point of the rare gases. In contrast, the melting point of fcc metals is found to be significantly lower, i.e., $kT_m/\varepsilon \approx 0.1$–$0.3$. Using the first neighbor EAM-LJ model, the melting point as a function of the amount of many-body bonding was calculated.

The calculation used the molecular dynamics technique of examining the motion of a solid/liquid interface to determine the melting point. This technique has the advantage of not having to nucleate either the liquid or the solid phase. We start with a cube of fcc material containing 2048 atoms of reduced mass 1, periodic in three dimensions. The interactions were truncated at a reduced distance of 1.4 using a method previously discussed [25]. The atoms were equilibrated at $kT/\varepsilon = 0.5$ and zero pressure for 1 unit of reduced time using Nose-Hoover temperature control [26,27], Parrinello-Rahman boundary conditions [28], and a time step of 0.001 in units of reduced time. Approximately half of the crystalline sample ($x > 0$) was then melted by increasing the temperature to $kT/\varepsilon = 2$ for 10 units of reduced time while keeping the atoms in the other half ($x < 0$) fixed. The periodic lengths in the y and z directions were held fixed, while the length in x was allowed to increase to allow the liquid to expand to maintain zero pressure. The radial distribution function of the high temperature region showed a characteristic liquid signature [3]. The thermostat of the whole sample was then set to various temperatures and the total energy was monitored for up to 30 units of reduced time. At a temperature above the melting point, the energy increased and the sample melted fully. Conversely at temperatures below the melting point the energy decreased and the whole sample ended up solid. Using this method it is easy to determine the melting point.

For the pure first neighbor LJ model ($A = 0$) the melting point was found to be given by $kT_m/\varepsilon = 0.52$ somewhat below the LJ melting point for a longer interaction range. We found that the LJ melting point increased to $kT_m/\varepsilon = 0.55$ when second neighbors were included. By scaling to the cohesive energy instead of the LJ bond energy, the melting points for both first ($kT_m/E_0 = 0.087$) and second neighbor interactions ($kT_m/E_0 = 0.082$) are found to be very close. Broughton and Gilmer [3] report a melting point of the LJ solid $kT_m/E_0 = 0.083$ for an interaction range of fourth neighbors, and Chokappa and Clancy [29] report $kT_m/E_0 = 0.084$ for the standard LJ seventh neighbor cutoff of $r_c/\sigma = 2.5$. These values are almost identical to the value reported here for second neighbor interactions.

The melting point was determined as a function of the many-body interactions for two values of β. The results are shown in Fig. 3. We see that the melting temperature decreases monotonically with increasing many-body interactions. In addition, there is a significant lowering

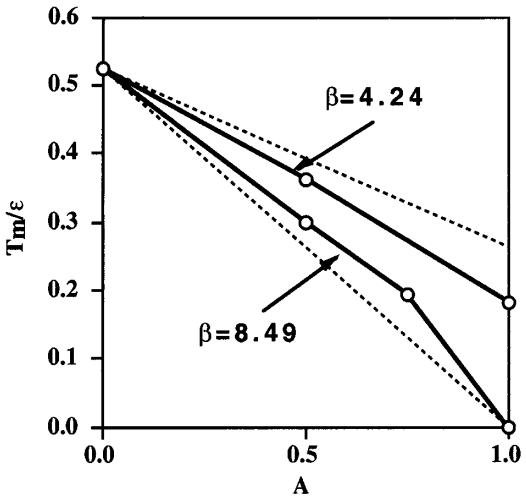

FIG. 3. Melting point (full lines) as a function of the model parameters A and β. Points actually calculated are shown by the symbols. The dashed lines show the decrease in the melting point expected if melting is controlled by shear.

of the melting point with increasing β. For the model with $\beta = 8.49$ and $A = 1$ the fcc structure is not stable relative to the liquid at any temperature. This instability may be understood by looking at the analytic expressions in Table I. Using these expressions we see that the shear elastic constants are zero, and the vacancy formation energy is less than zero. The decrease with melting point may be understood by examining the dependence of the shear elastic constants with model parameters. From Table I we see that c_{44} at 0 K decreases as $1 - A\beta^2/72$. If melting is controlled by shear processes, we would expect that the melting point would be proportional to the shear modulus. This dependence is shown in the figure and it is seen that the calculated melting point scales quite well with the value of the shear modulus at room temperature. Of course, the shear modulus itself decreases with temperature. This effect could lead to an additional lowering of the melting point. In contrast, if melting were controlled by vacancy formation, we would expect the melting point to be independent of β and to follow a curve similar to the lower dashed line in Fig. 3. Models of melting have been developed based on shear instability [30,31] and excess vacancies [32]. The EAM-LJ model is more consistent with the shear instability model.

This work was supported by the U.S. DOE.

*Current address: Los Alamos National Laboratory, Los Alamos, NM 87545.

[1] J. E. Lennard-Jones, Proc. R. Soc. London A **106**, 463 (1924).
[2] E. J. Jensen, W. D. Kristensen, and R. M. J. Cotterill, Philos. Mag. **27**, 623 (1973).
[3] J. Q. Broughton and G. H. Gilmer, J. Chem. Phys. **79**, 5095 (1983).
[4] W. C. Swope and H. C. Andersen, Phys. Rev. B **41**, 7042 (1990).
[5] B. W. v. d. Waal, Phys. Rev. Lett. **67**, 3263 (1991).
[6] P. R. t. Wolde, M. J. Ruiz-Montero, and D. Frenkel, Phys. Rev. Lett. **75**, 2714 (1995).
[7] Y. C. Shen and D. W. Oxtoby, Phys. Rev. Lett. **77**, 3585 (1996).
[8] M. Dzugutov, Nature (London) **381**, 137 (1996).
[9] W. Kob, C. Donati, S. J. Plimpton, P. H. Poole, and S. C. Glotzer, Phys. Rev. Lett. **79**, 2827 (1997).
[10] C. Donati, J. F. Douglas, W. Kob, S. J. Plimpton, P. H. Poole, and S. C. Glotzer, Phys. Rev. Lett. **80**, 2338 (1998).
[11] J. Q. Broughton and G. H. Gilmer, J. Chem. Phys. **9**, 5105 (1983).
[12] R. M. J. Cotterill, T. Leffers, and H. Liltholt, Philos. Mag. **30**, 265 (1974).
[13] F. F. Abraham, D. Brodbeck, W. E. Rudge, and X. P. Xu, J. Mech. Phys. Solids **45**, 1595 (1997).
[14] R. Mikulla, J. Stadler, F. Krul, H.-R. Trebin, and P. Gumbsch, Phys. Rev. Lett. **81**, 3163 (1998).
[15] A. E. Carlsson, *Beyond Pair Potentials in Elemental Transition Metals and Semiconductors* (Academic Press, Boston, 1990).
[16] M. S. Daw and M. I. Baskes, Phys. Rev. Lett. **50**, 1285 (1983).
[17] M. S. Daw and M. I. Baskes, Phys. Rev. B **29**, 6443 (1984).
[18] M. S. Daw, S. M. Foiles, and M. I. Baskes, Mater. Sci. Rep. **9**, 251 (1993).
[19] B. L. Holian, A. F. Voter, N. J. Wagner, R. J. Ravelo, S. P. Chen, W. G. Hoover, C. G. Hoover, J. E. Hammerberg, and T. D. Dontje, Phys. Rev. A **43**, 2655 (1991).
[20] M. I. Baskes, Phys. Rev. B **46**, 2727 (1992).
[21] L. Pauling, *The Nature of the Chemical Bond* (Cornell University Press, Ithica, NY, 1960).
[22] M. I. Baskes, Phys. Rev. Lett. **59**, 2666 (1987).
[23] P. J. Craievich, M. Weinert, J. M. Sanchez, and R. E. Watson, Phys. Rev. Lett. **72**, 3076 (1994).
[24] J. A. Pryde, *The Liquid State* (Hutchinson University Library, London, 1969).
[25] M. I. Baskes, Mater. Chem. Phys. **50**, 152 (1997).
[26] W. G. Hoover, Phys. Rev. A **31**, 1695 (1985).
[27] S. Nose, Prog. Theor. Phys. Suppl. **103**, 1 (1991).
[28] M. Parrinello and A. Rahman, J. Appl. Phys. **52**, 7182 (1981).
[29] D. Chokappa and P. Clancy, Mol. Phys. **61**, 617 (1987).
[30] M. A. Durand, Phys. Rev. **50**, 449 (1936).
[31] M. Born, J. Chem. Phys. **7**, 591 (1939).
[32] T. Górecki, Scr. Metall. **11**, 1051 (1977).